

Unsupervised Calibration for Multi-beam Lasers

Jesse Levinson, Sebastian Thrun
Stanford Artificial Intelligence Laboratory
{jessel,thrun}@stanford.edu

Abstract—Keeping pace with technological progress, robot sensors are generating increasing amounts of data; a particular recent trend has been a shift from single-beam LIDAR sensors to multi-beam versions. Whereas single-beam sensors can often be calibrated without great difficulty, deriving an accurate calibration for lasers with many simultaneous beams has been a tedious and significantly harder challenge. In addition, existing calibration methods require specific and known environmental features.

Instead, we propose a fully unsupervised approach to multi-beam laser calibration. We attempt to recover optimal parameters for each beam’s orientation and distance-response function as well as a fully probabilistic generative model for each beam’s remittance response to surfaces of varying reflectivity. Our method allows simultaneous calibration of tens or hundreds of beams, each with its own parameters. In addition, we recover the sensor’s extrinsic pose relative to the robot’s coordinate frame.

Crucially, our approach requires no specific calibration target, instead relying only on the weak assumption that points in space tend to lie on contiguous surfaces. Specifically, we define an energy function on point clouds that penalizes points far away from surfaces defined by points from other beams. Then, by aggregating points acquired across a series of poses, we take derivatives of the energy function across pairs of beams with respect to individual parameters. Using an iterative optimization method we arrive at a globally consistent calibration with very low error.

Demonstrating our algorithm with a 64-beam LIDAR unit on a moving vehicle equipped with an IMU, we show that we can precisely solve for the LIDAR’s extrinsic pose and derive accurate 192-parameter orientation and distance calibrations even from grossly inaccurate initializations and without any calibration target or environment measurements. We also show significant improvements to the resulting remittance environment maps resulting from these calibrated parameters as well as the learned Bayesian model for each beam’s remittance response.

I. INTRODUCTION

Light Detection and Ranging (LIDAR) sensors have become increasingly common in both industrial and robotic applications. LIDAR sensors are particularly desirable for their direct distance measurements and high accuracy, but traditionally have been configured with only a single rotating beam. However, recent technological progress has spawned a new generation of LIDAR sensors equipped with many simultaneous rotating beams at varying angles, providing at least an order of magnitude more data than single-beam LIDARs and enabling new applications in mapping [6], object detection and recognition [15], scene understanding [16], and SLAM [9].

In order to effectively harness this massive increase in beam count, new calibration methods are required. First, calibrating angles and range readings for tens or hundreds of beams

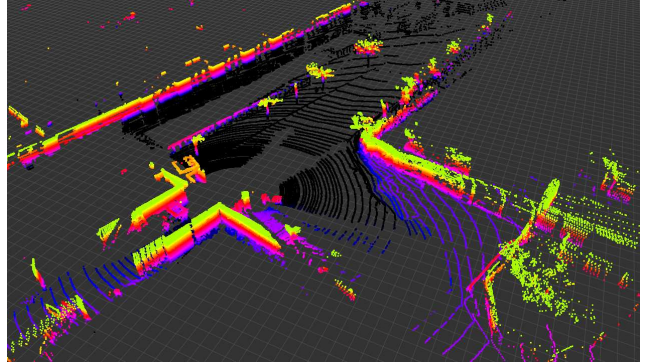


Fig. 1. A single 360-degree scan from the 64-beam Velodyne LIDAR. Points are colored by height for visual clarity.

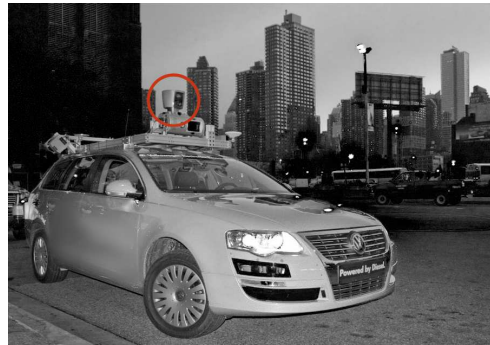


Fig. 2. Our vehicle platform. Velodyne LIDAR unit is circled in red.

is a substantially harder problem than calibrating one or a few beams. Second, for applications that utilize the intensity returns of LIDAR sensors, e.g. recent mapping and localization work [6], it is important that the intensity remittance values agree across beams. In both cases, the number of parameters makes supervised measuring and calibration at best tedious and at worst infeasible.

To date, there has been limited research on supervised calibration for multi-beam LIDARs. The most popular such unit as of this writing is the Velodyne HD-64E spinning LIDAR, which has been used extensively for many recent robotics applications. A representative scan from such a sensor is shown in Fig. 1. In [4], the authors present a supervised calibration technique for this LIDAR requiring a dedicated calibration target and many hand measurements, followed by a traditional optimization step. Indeed, the manufacturers of this laser built a dedicated calibration facility which they use to collect thousands of measurements followed by an unpublished

optimization routine, in order to provide a calibration of each beam to the customer.

In the case of single-beam LIDARs, there have been attempts at unsupervised recovery of roll, pitch, and yaw in a known rectangular enclosure [2] as well as an attempt to estimate the noise parameters of a single-beam LIDAR [3]. Recent work has provided algorithms for calibrating one [10] or two [1] single-beam LIDARs on a moving vehicle platform using hand-placed retroreflective calibration targets, which additionally requires an intensity threshold for correspondences.

None of these techniques extends to the unsupervised calibration of a multi-beam LIDAR. Indeed, we are unaware of any algorithm in the literature to date that is able to recover the extrinsic pose of any LIDAR unit relative to a vehicle frame when it is the only such sensor on the vehicle and when the environment has no particular known features. In addition, we are similarly unaware of an existing algorithm that calibrates individual beam parameters for multi-beam units without hand-measured environmental features.

Although hand measurements are practical in some cases for single-beam sensors, especially for translational offsets, it is particularly difficult to measure sensor orientation with high accuracy in the absence of a dedicated calibration environment. Furthermore, for sensors with many beams, such measurements may take prohibitively long and would inevitably be suboptimal in accuracy. Finally, techniques that require specifically placed retroreflective targets with careful thresholding to pick them apart from the rest of the environment are not applicable in all settings a robot might encounter; they also result in the consideration of only a tiny fraction of the available data.

Thus, we propose a novel fully unsupervised extrinsic and intrinsic calibration method for multi-beam LIDAR sensors that requires no calibration target, no labeling, and no manual measurements. Given a multi-beam LIDAR attached to a moving platform or robotic vehicle along with accompanying inertial measurement unit (IMU) readings, our algorithm computes hundreds of sensor parameters from only seconds of data collected in an arbitrary environment without a map.

Our contribution consists of three complimentary unsupervised calibration algorithms. The first discovers the LIDAR's extrinsic 6-dimensional pose relative to the vehicle's inertial frame, including translation and rotation. The second estimates optimal vertical and horizontal angles for each individual beam and an additive distance offset for each beam's range reading. Finally, the third derives a fully Bayesian generative model for each beam's remittance intensity response to varying surface reflectivities in the environment.

In the sections that follow, we will describe each of the above algorithms conceptually. We will then provide details about our particular implementation of these techniques on a ground vehicle with a roof-mounted 64-beam rotating LIDAR, along with several results demonstrating the effectiveness of these algorithms even when presented with poor initial calibrations. Finally, we will discuss implications for related applications and possible extensions for future research.

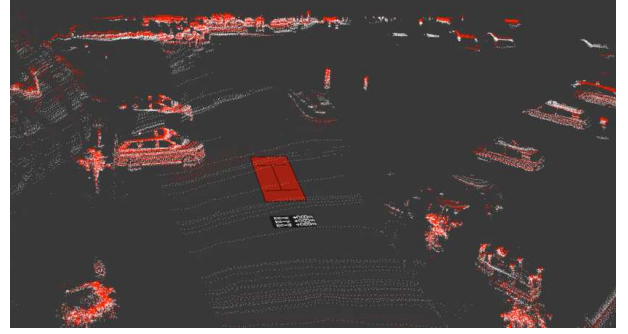


Fig. 3. Velodyne points from two adjacent beams (of 64) accumulated over time and projected into 3D; one beam colored red, the other white. Due to known vehicle motion, both beams tend to see the same surfaces.

II. EXTRINSIC CALIBRATION

In the case of a multi-beam LIDAR, extrinsic calibration considers the mounting location of the entire unit relative to the vehicle's own coordinate frame, while intrinsic calibration considers the configuration of each individual beam inside the unit. In this section we present a method for extrinsic calibration, assuming a known intrinsic calibration.¹

At the most basic level, our approach for both calibrations leverages the simple observation that laser returns projected into three dimensions are not randomly distributed in space. Indeed, because the returned points are reflections off of physical surfaces, it is impossible for a properly calibrated sensor traveling a known trajectory to return a collection of accumulated points that is randomly distributed in three dimensions. As such, the proposed method relies only on the weak assumption that points in space tend to lie on contiguous surfaces.

Consider Fig. 3, which depicts LIDAR returns from just two adjacent beams accumulated over several seconds of vehicle motion along a known trajectory. Here, we color one beam in red and the other in white; it is apparent that due to the LIDAR's movement through space, to a large extent both beams end up hitting the very same surfaces.

The location of the LIDAR unit relative to the vehicle's coordinate frame will be expressed with an x (longitudinal), y (lateral), and z (height) offset along with roll, pitch, and yaw angles. The $(0, 0, 0)$ reference point and reference orientation is specified by the coordinate system being used, i.e. the three-dimension point and orientation that the vehicle's positioning system considers to be the origin.

In contrast to existing methods, our approach makes no assumptions about the environment other than that it is generally static and contains some 3D features, i.e. is not just smooth ground. In order to achieve an accurate calibration, we record LIDAR measurements as the vehicle transitions

¹If neither the extrinsic nor intrinsic calibration is known precisely, then the two separate calibration procedures can be performed iteratively until both converge.

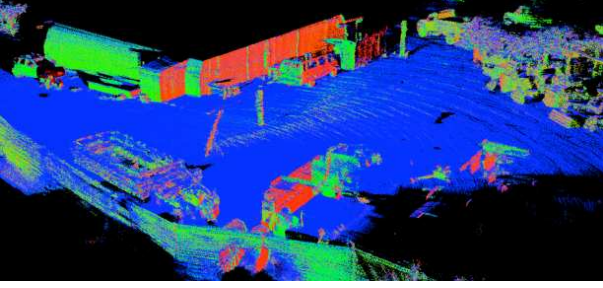


Fig. 4. Accumulated points colored by computed surface normal; the red, green, and blue channels respectively are set to the surface’s x, y, and z components of the normal vector at each point.

through a series of known poses.² Global pose information is irrelevant, as there is no existing map, so only local pose information is required. Local pose data may be acquired in any number of ways, e.g. from a wheel encoder and IMU, from an integrated GPS/IMU system, or from a GPS system with real-time corrections. Again, it is only the relative motion of the vehicle through the trajectory that is relevant to the calibration, so no global pose data is necessary.

Now, we define an energy function on point clouds which penalizes points that are far away from surfaces defined by points from other beams:

$$J = \sum_{b_i=1}^B \sum_{b_j=b_i-N}^{b_i+N} \sum_k w_k \|\eta_k \cdot (p_k - m_k)\|^2$$

where B is the total number of beams and N is the number of neighboring beams we align each beam to, k iterates over the points seen by beam b_j , p_k is the k th point projected according to the current transform, m_k is the closest point to p_k seen by beam b_i , η_k is the surface normal at point m_k and w_k is 1 or 0 based on whether $\|p_k - m_k\| < d_{max}$

This energy function bears similarity to the point-to-plane iterated closest point (ICP) error function [7], with two key differences. First, we compare surfaces defined by points in each beam individually against points in neighboring beams. This has the crucial benefit that an erroneous calibration between beams will not significantly affect surface normals in the set of points seen by any individual beam. Second, unlike in ICP, we are not dealing with rigid point clouds, as a change in any calibration parameter will transform the points in that beam’s point cloud in a complex way, since in this case the points in each cloud were observed at different times and thus from different poses of the sensor.

Surface normals are computed separately per beam, by fitting a plane to each point’s 20 nearest neighbors in the accumulated projected points from the entire trajectory. Due

to the density of data from multi-beam LIDARs, this local neighborhood for each point is very small. We show an example of these surface normals in Fig. 4, where the red, green, and blue channels are colored according to normal vector’s x, y, and z components at each point.

A further benefit of the high density of points returned by multi-beam LIDARs is that almost any surface will be nearly locally planar at the resolution of the pointcloud; thus, projecting points from one beam onto the surfaces defined by points in neighboring beams results in very low errors when all calibrations are accurate.

Given the above energy function, all that remains is to select the extrinsic calibration that minimizes the total score. Although in theory the objective is not necessarily convex, and thus finding the true global optimum cannot be guaranteed in any reasonable amount of time, in practice the energy function is quite smooth and standard search heuristics perform very well.

In our approach, we alternatively optimize the translation parameters and rotation parameters until both have converged. For each optimization, we utilize grid search, which compares the current energy score with the score that results from adjusting the variables in question in all possible directions jointly. Whereas a coordinate descent iteration takes time linearly proportional to the number of variables, grid search takes time exponential in the number of variables, as it considers all combinations of directions. As a result, it is less prone to getting stuck in local minima, and as neither translation nor rotation individually has more than three variables, grid search is computationally tractable. For example, when considering a rotation change, each of roll, pitch, and yaw can be increased, held constant, or decreased, which results in 26 new comparisons to the current score.³

We start with a relatively large step size, iterate until convergence, and repeatedly reduce the step size until we’ve reached the finest granularity we desire. At the end of the last optimization, we obtain our final calibration parameters.

III. INTRINSIC CALIBRATION OF EACH BEAM

The motivation in the previous section applies equally to the case of intrinsic calibration. That is, an intrinsic calibration that computes each beam’s horizontal and vertical angle and range offset correctly will necessarily yield a lower energy score than an incorrect calibration.

It is worth emphasizing that this property is a direct consequence of the fact that the vehicle moves during data collection. For a stationary vehicle, it is impossible to disambiguate certain calibrations; indeed, many possible angles and range offsets may be equally plausible in that case. But when the vehicle moves in a known trajectory, no longer will incorrect

²The vehicle trajectory can be arbitrary, but must include a change in yaw so that lateral and longitudinal offsets of the LIDAR can be detected; if the vehicle only moves straight, these cannot be disambiguated. Similarly, we do not attempt to recover the sensor’s height, as our vehicle always remains nearly parallel to the ground, though height can trivially be determined by considering the distance to points the vehicle drove over.

³It is important to note that for every possible calibration considered, all points must be reprojected into 3D space based on the vehicle’s pose at the time each point was acquired. Thus, a calibration change does not warp or distort all points in the same way, as the effect of a calibration change on each individual point depends on where the vehicle was at the time that return was measured.

calibrations result in plausible pointclouds when each beam's returns are accumulated over time and projected appropriately into 3D space.

Although the energy function used to calibrate the sensor's extrinsic pose is equally applicable to its intrinsic calibration, it is intractable to perform grid search over 3 parameters for each of tens or hundreds of beams jointly. Instead, we alternately consider all horizontal angles, all vertical angles, and all range offsets until convergence. At each step, for the variables in question, we take empirical derivatives of the energy function across pairs of beams with respect to the individual parameters. Consider again the energy function:

$$J = \sum_{b_i=1}^B \sum_{b_j=b_i-N}^{b_i+N} \sum_k w_k \|\eta_k \cdot (p_k - m_k)\|^2$$

At each iteration, for each beam b_i and neighboring beams b_j we hold fixed the accumulated projected pointclouds and accompanying surface normals associated with beam b_j and then re-project the points from beam b_i with the parameter in question increased and then decreased by some increment α . For each of the two possibilities, the inner part of the energy function, $\sum_k w_k \|\eta_k \cdot (p_k - m_k)\|^2$ is recomputed; the parameter is then changed by α in whichever direction improves the objective maximally, or else the parameters is held constant if any perturbation is worse.

In this manner, we iteratively loop through all parameters and beams, optimizing the objective function at each step, until either some predetermined number of iterations is reached or until the change in the global objective function becomes sufficiently small. We note that although this heuristic works well in practice, unlike with grid search for extrinsic calibration, it is not actually guaranteed to lower the objective function in any given iteration, as it updates a particular parameter for all beams in each iteration. Given the extremely large search space, however, such approximations are reasonable, and, as we show in the results section, work very well in practice.

IV. REMITTANCE CALIBRATION

In addition to estimating the LIDAR's pose and beam parameters, we also derive a Bayesian generative model of each beam's response to surfaces of varying reflectivity using Expectation Maximization. [8]

As the vehicle transitions through a series of poses, let T be the set of observations $\{z_1, \dots, z_n\}$ where z_i is a four-tuple $\langle b_i, r_i, a_i, c_i \rangle$ containing the beam ID, range measurement, intensity measurement, and map cell ID of the observation, respectively. The map may be comprised of 2D cells in which points are projected to the ground plane, or full 3D correspondences can be used. As we have shown in previous work [6], the deterministic calibrated output $c(a, j)$ of beam j with observed intensity a can be computed in a single pass as follows:

$$c(j, a) := \mathbb{E}_{z_i \in T} [a_i \mid ((\exists k : c_i = c_k, b_k = j, a_k = a), b_i \neq j)]$$

That is, the calibrated output when beam j observes intensity a is the conditional expectation of all other beams'

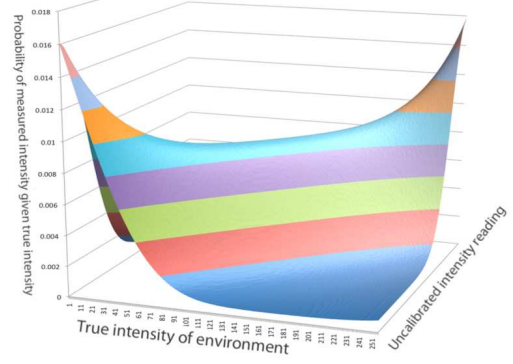


Fig. 5. Bayesian prior for beam remittance response function as a function of surface intensity, used to initialize EM.

intensity readings for map cells where beam j observed intensity a .

Taking this further, we can derive a probabilistic calibration that specifically models the uncertainty and noise characteristics of each beam, which in practice are often very different. We note that although environment reflectivity is of course continuous, for computational reasons we restrict the values to integers between 0 and 255, as this matches the range of the Velodyne's returns. Thus for each map cell c_i we maintain a distribution $P(m)$ indicating the probability that map cell c_i has intensity m , for $m = 0$ to 255.

Now, for each beam b_i we wish to estimate a distribution $P(a_i|m)$ indicating the probability that beam b_i will return intensity a_i given that cell c_i has intensity m . Each map cell is initialized with a uniform intensity prior, and for each beam we initialize the prior

$$P(a|m) = \eta \cdot \exp\left(-\frac{(a-m)^2}{\tau}\right) + \varepsilon$$

where η is the normalizer, τ controls the peakiness of the distribution, and ε affords a nonzero probability of a random intensity return. With this initialization, *a priori* beams are likely to return values near the true brightness of the map, as shown in Fig. 5.

Starting with the initializations above we then alternate between computing $P(m)$ for each map cell (E-step) and computing $P(a_i|m)$ for each beam and map intensity (M-step). We note that while the intensities of each map cell are by no means independent, because they are jointly affected by the beam models, they are conditionally independent of each other given the beam models, which allows us to apply EM. The update equations are as follows:

E-step:

$$P(m_k = m) = \eta \cdot \prod_{i:c_i=k} P(a_i|m; b_i)$$

Thus, in the Expectation step we compute the distribution over intensities for each map cell given the current beam parameters.

M-step:

$$P(m|a;b) = \eta \cdot \sum_{k=1}^K P(m_k = m) \cdot \mathbf{1}\{\exists i : b_i = b, c_i = k, a_i = a\}$$

$$P(a|m;b) = \eta \cdot P(m|a;b) \cdot P(a)$$

Thus, in the Maximization step we compute the most likely beam parameters given our observed data and our current distribution over the intensities for each map cell. First we compute the probability of each map cell having all possible intensities given the observed intensity return for that cell by each beam and the distribution over intensity values for that cell as computed in the E-step. Then, using Bayes' rule we compute the distribution over possible intensity return values for each beam given the distribution over the map cell intensities.

After EM converges, we have a fully generative model for each beam's response to environment surfaces of different reflectivities.

V. EXPERIMENTAL RESULTS

We demonstrate the performance of the calibration algorithms presented here with several experiments. We used a Velodyne HD-64E S2 LIDAR sensor with 64 beams oriented between -22 to +2 degrees vertically and rotating 360 degrees horizontally. The unit spins at 10Hz and provides around 100,000 points per spin. This sensor was mounted to the roof of our research vehicle as shown in Fig. 2.

In addition, our vehicle pose was provided by an Applanix LV-420 positioning system that combines GPS, IMU, and wheel encoder readings to provide global and inertial pose updates at 200 Hz. However, as the methods described here only require locally consistent pose data, we ignored the global GPS pose values and only used the unit's local 6-DOF velocity updates, which we integrated over time to produce a smooth local coordinate frame.

We implemented our algorithms in C, taking advantage of the University of Maryland's Approximate Nearest Neighbor (ANN) library [5]. For the following results, we used a maximum matching distance of 20cm and generated per-beam pointclouds and surface normals using all laser returns, but only evaluated the energy function at every 16 points for efficiency; with over a million points returned by the Velodyne per second, it is unnecessary to evaluate the energy function at every single point. With this implementation on a modern desktop processor, using about 15 seconds of recorded data, the extrinsic and intrinsic calibrations each take on the order of one hour to converge, given a very bad initialization. The remittance intensity calibration is faster, requiring a few minutes to run.

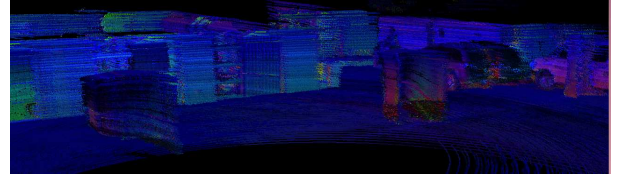
A. Extrinsic calibration

First, we show that we can precisely and reliably compute the Velodyne's mounting location on our vehicle, even with a poor initialization. As discussed previously, we attempt to recover the sensor's lateral and longitudinal offset and roll, pitch, and yaw relative the the vehicle's coordinate frame.



Fig. 6. Initial Velodyne mounting position (left) and after translation and rotation (right)

(a) Assuming previous Velodyne position.



(b) After calibrating for the updated position

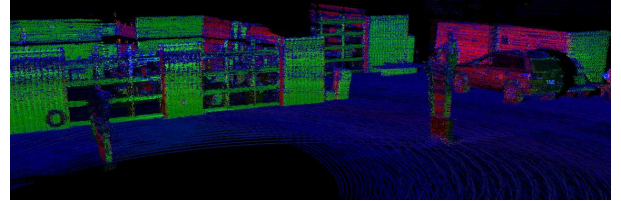


Fig. 7. Moving and rotating the Velodyne, but continuing to use the original position calibration, projecting accumulated Velodyne points into 3D results in massively deformed structures and significant blurring of surfaces (a). After calibration (b), the points are much better aligned, and the computed transform for the Velodyne is extremely accurate.

We collected two short 15-second logfiles with each of two different mounting positions for the Velodyne, for a total of four logfiles. In all four cases, we drove the vehicle in a tight semi-circular arc close to a building at 2 m/s.

First, we ran the calibration routine on the two logfiles taken with the initial mounting position. Here, the Velodyne sensor was centered laterally on the vehicle, and positioned 1.51 meters forward of the rear axle, which is our positioning system's reference origin. It was pointed straight forward and mounted parallel to the roof rack, as shown in Fig. 6 (left).

On the first logfile, starting with an initial calibration that was within 10cm and 1° of the measured location, our algorithm computed a lateral position of 0.00m, a longitudinal position of 1.51m, a roll of -0.03°, a yaw of 0.00°, and a pitch of -0.46°. On the second logfile, with the Velodyne in the same location, the algorithm computed a lateral position of -0.01m, a longitudinal position of 1.50m, a roll of -0.03°, a yaw of 0.03°, and a pitch of -0.46°. Thus, from two separate drives, from two different locations, the resulting position estimates

were within 1 cm and $.03^\circ$ of each other in all dimensions.⁴

For a more challenging test, we then remounted the Velodyne 5.6 cm to the right and 20.6 cm behind the original location, and we rotated it counter-clockwise (around the Z axis) by 9 to 10° , as shown in Fig. 6 (right). Now, starting with the calibrated pose from the original mounting location, we ran our algorithm on each of the two new logfiles. On the second of the new logfiles, it correctly estimated that the sensor had been moved by 6 cm to the right and 21 cm to the rear, and rotated by 9.78° counter-clockwise. The dramatic improvement in the resulting 3D pointcloud, comparing the assumed original mounting location to the estimated new location, is shown in Fig. 7.

On the first of the new logfiles the estimate was less accurate; the computed offsets were 16cm to the right and 30cm to the rear, along with 9.56° counter-clockwise. Thus, although the directions of the movement were correct, the amounts were not. Upon examining this logfile, we discovered that there had in fact been IMU drift across the trajectory, which resulted in the accumulated 3D pointcloud showing visible smearing. Indeed, the inaccurate Velodyne pose estimate our algorithm computed not only had a better scoring energy function than the correct calibration for that logfile, but it also visually resulted in less smearing than the correct calibration. In this case, our algorithm picked the extrinsic calibration that resulted in the "best" 3D pointcloud, but because the assumption of a correct local trajectory was violated, the estimated calibration was a bit off.

Therefore, these results demonstrate that our algorithm produces extremely accurate extrinsic pose estimates when the trajectory is known precisely, and that its performance degrades when the trajectory estimate is inaccurate.

B. Intrinsic calibration

Next, we show that we can accurately calibrate the Velodyne sensor's individual beam angles and range offsets. Recent improvements in Velodyne's meticulous supervised factory calibration give better results than earlier models; not only can our algorithm do better still, we show that we are able to take an artificially bad calibration and use our methods to arrive at a calibration whose accuracy exceeds the best available factory calibration. Fig. 8 depicts such an optimization; starting with an unrealistically bad calibration in which we set all horizontal angles to be 0 and all range offsets to be equal,⁵ we are able to recover an excellent calibration based on only 10 seconds of data in a complex unlabeled environment.

We show quantitative success in two ways. First, in optimizing the intrinsic calibration, the angles and range offsets we compute are very similar to the factory values, even when

⁴We are only able to measure the mounting angles to within 1° , so we cannot empirically verify the angle calibration to within the $.03^\circ$ granularity to which we estimate angles in our algorithm; however, both the energy functional and the surfaces in the resulting 3D pointclouds are optimal with the computed calibration and degrade noticeably if they are changed in either direction.

⁵In reality, the horizontal beam angles range from -9° to $+9^\circ$ within the Velodyne and the range offsets range from 0.85m to 1.53m.

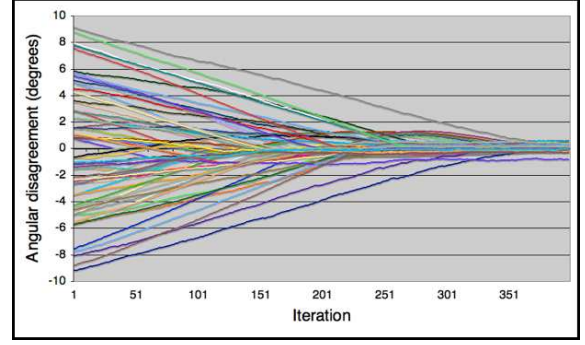


Fig. 9. Comparing the horizontal angles of all 64 beams with the factory calibration, starting with a uniform initial estimate and optimizing over 400 iterations. Here, the update step size was very low for clarity. Initially beams were miscalibrated by up to 9° , and after calibration all beams' angles agreed with the factory calibration to within 1° , with an RMS deviation of only $.25^\circ$.

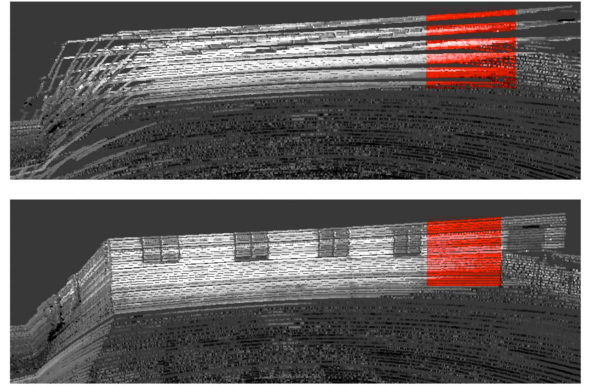


Fig. 10. Improvement in wall planarity with calibration.

initialized to be significantly different. In one experiment, we optimize the horizontal angles starting from a uniform initial estimate of 0° per beam. With this initialization, the beam angles disagree with the factory calibration by up to 9° , with an RMS disagreement of 4.6° ; after our optimization, the maximum disagreement is less than 1° , with an RMS disagreement of 0.25° (Fig. 9). Thus our result is, for all beams, very similar to the factory calibration. Indeed, although we are unable to measure angles to these tolerances, we find the resulting energy functional and visual appearance of our calibration both outperform the factory calibration, suggesting that much of the disagreement may be due to factory miscalibration, or slight angle shifting over time.

Going further, in Fig. 10 we see another application of our calibration in a simpler environment, after which we hand-selected an area of horizontal ground and vertical wall known to be planar, and in Fig. 11 we compare the RMS distance of the points to their approximating plane over the course of optimization. With our artificially bad calibration we start with ground and wall errors of 54 and 4 cm, respectively, and after optimization these are reduced to 4 and 2 cm, respectively. Importantly, the baseline Velodyne factory calibration gives errors of 6cm and 3cm, respectively, so our unsupervised method provides superior results.

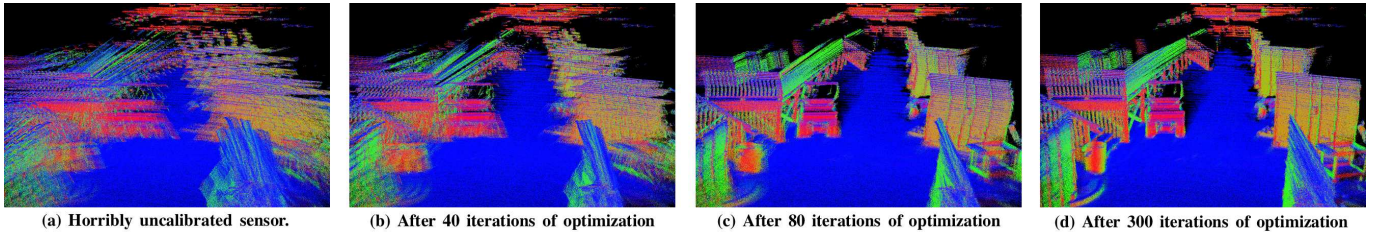


Fig. 8. Unsupervised horizontal angle and range calibration using 10 seconds of data (all scans depicted above). Points colored by surface normal. Even starting with an unrealistically inaccurate calibration (a) we are still able to achieve a very accurate calibration after optimization (d).

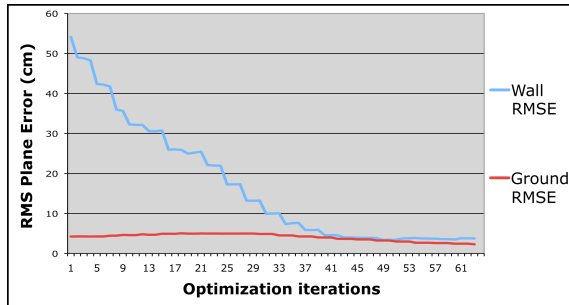


Fig. 11. Quantitative improvement in wall planarity during calibration procedure. Final result exceeds factory calibration for both wall and ground.

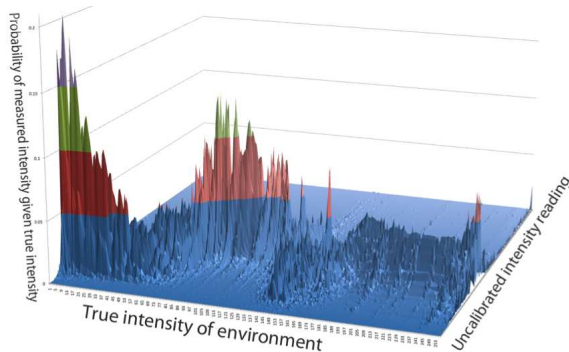


Fig. 12. The learned generative model $P(a_i|m)$ for beam 37 of 64.

C. Bayesian remittance calibrations

The results of Bayesian intensity calibration can be seen in Fig. 12, in which we plot the learned generative model for one of the 64 beams. Here we see, as expected, that brighter surfaces tend to yield brighter returns. The somewhat surprising non-monotonicity of the graph corresponding to the brightest 45% of surfaces may be partially explained by the fact that fewer than 0.1% of the Velodyne returns fall into that brightness region. Thus, there is very little data to generate that section of the graph; at the same time, this phenomenon causes that region of the response function to rarely be queried.

Each beam has a significantly different intensity response; we show the expected intensity values of the environment given each beam’s measured intensity in Fig. 13.

Finally, we show the significant impact of angle, range, and intensity calibration on the resulting laser maps. In Fig. 14 we show an orthographic intensity map of points projected

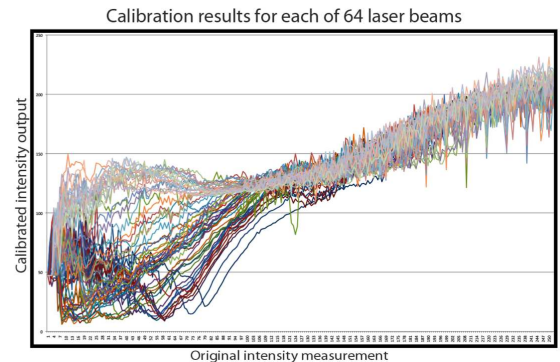


Fig. 13. The expected environment intensity given each beam’s intensity return. All 64 beams are shown here; note significant variation between beams.

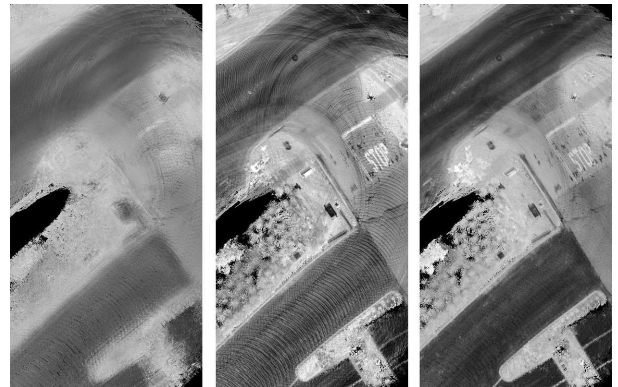


Fig. 14. Improvement from calibration. We compare an orthographic intensity map of a street with the horrible angle and range calibration used in Fig. 8 (left), the same map with the learned angles and ranges (center), and finally adding intensity calibration (right). The final result is much improved.

to the ground plane, first with our artificially bad calibration, then with calibrated angles and ranges, and lastly adding calibrated intensities. The final calibrated map displays excellent sharpness and contrast, indicative of a well-calibrated sensor.

VI. CONCLUSION

Multi-beam LIDAR sensors are a key enabling component of advanced mapping and robotic applications, and their use will only increase with time. We have presented what we believe to be the first complete fully unsupervised calibration algorithms for these sensors, and have demonstrated that ex-

cellent results are achievable with a trivial amount of data collection in arbitrary unlabeled environments even with terrible initializations. In addition, these methods are extensible and have many related applications. For example, these algorithms could easily be extended to the calibration of multiple single-beam LIDARs mounted to one vehicle platform.

Due to the particularly large amount of data generated and extremely large search space, the algorithms discussed here are naturally suited to be run offline. However, it is conceivable that with intelligent data pruning and more aggressive search techniques, a similar realtime algorithm could be developed to enable on-the-fly sensor calibration while driving. For most applications, offline calibration is sufficient, but for sensors that are unable to be perfectly secured to the vehicle, a realtime algorithm would provide some benefits.

Although the algorithms we discuss here make particularly few assumptions about the environment, they do treat the environment as static, i.e. we assume it is only the data collection vehicle that is moving. To the extent that there are dynamic obstacles during data collection, this motion could interfere with the results; in these cases, existing segmentation and tracking algorithms could be employed [12, 13] to remove such tracks, although an especially poor initial calibration may render segmentation and tracking more difficult than usual.

In this paper we presented a solution to a particular instance of the Simultaneous Calibration and Mapping (SCAM) problem, in which neither a calibration nor a map is available *a priori*. Such situations are in fact common in practice, despite being significantly less studied than the more popular Simultaneous Localization and Mapping (SLAM) problems. This discrepancy is perhaps due in part to the fact that reasonable calibrations for simple sensors are often obtainable by hand measurement, whereas SLAM problems cannot be solved similarly. In addition, SCAM - or at least the solution presented here - is inapplicable to single-beam sensors as they alone do not provide enough data for fully unsupervised calibration in the general setting.

A natural extension would be to combine SCAM with SLAM; that is, to solve Calibration, Localization, and Mapping jointly when none are known precisely. In preliminary work, we have aligned a several-minute logfile with both SLAM and SCAM as presented here; a resulting 3D pointcloud can be seen in Fig. 15. However, more research is required to arrive at a consistent approach to jointly optimizing all unknowns in the general case, particularly if the initial pose estimate is poor. Our results benefit from a high-end IMU, which is not available or practical for all robots, and thus a joint algorithm for recovering calibration and localization without a known map would be a worthwhile goal for future research.

REFERENCES

- [1] G. Chao and J. Spletzer "On-Line Calibration of Multiple LIDARs on a Mobile Vehicle Platform." ICRA 2010.
- [2] A. Censi, L. Marchionni, and G. Oriolo "Simultaneous maximum-likelihood calibration of odometry and sensor parameters." ICRA 2008.

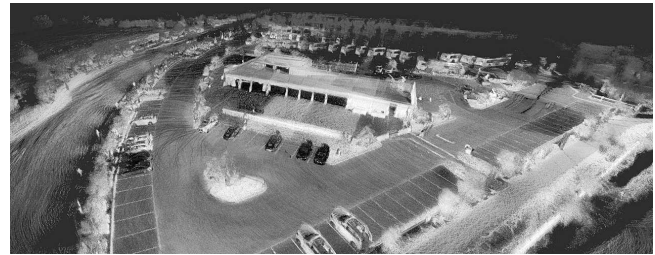


Fig. 15. 3D pointcloud of a campus parking lot after SLAM and calibration; 60 seconds of accumulated data colored by intensity return.



Fig. 16. Closeup from above scene from another perspective; points colored by both intensity return and surface normal.

- [3] A. Kaboli, M. Bowling, and P. Musilek "Bayesian calibration for Monte Carlo localization." AAAI 2006.
- [4] N. Muhammad and S. Lacroix "Calibration of a rotating multi-beam Lidar" published on-line at <http://www.pgcs.fr/2rt3d/SortedDocs/Publications/MultiBeamLidar2.pdf> 2009.
- [5] D. Mount and S. Arya "ANN: A Library for Approximate Nearest Neighbor Searching" available on-line at <http://www.cs.umd.edu/mount/ANN/>
- [6] J. Levinson and S. Thrun "Robust Vehicle Localization in Urban Environments Using Probabilistic Maps" ICRA 2010.
- [7] Y. Chen and G. Medioni "Object Modeling by Registration of Multiple Range Images" Proc. of the 1992 IEEE Intl. Conf. on Robotics and Automation, pp. 2724-2729, 1991.
- [8] A. Dempster, P. Laird, D. Rubin "Maximum likelihood from incomplete data via the EM algorithm." Journal of the Royal Statistical Society. Series B 39(1): 1-38.
- [9] A. Segal, D. Haehnel, and S. Thrun "Generalized-ICP" Robotics Science and Systems, 2009.
- [10] J. Underwood, A. Hill, and S. Scheduling "Calibration of range sensor pose on mobile platforms" in Proceedings of the 2007 IEEE/RSJ International Conference on Intelligent Robots and Systems, San Diego, CA, October 2007
- [11] S. Thrun, W. Burgard and D. Fox. Probabilistic Robotics. MIT Press, 2005.
- [12] K. Lee, B. Kalyan, S. Wijesoma, M. Adams, F. Hover, and N. Patrikalakis "Tracking random finite objects using 3D-LIDAR in marine environments" Proceedings of the 2010 ACM Symposium on Applied Computing.
- [13] J. Shackleton, B. VanVoorst, J. Hesck "Tracking People with a 360-degree Lidar" 7th IEEE Conference on Advanced Video and Signal Based Surveillance. 2010.
- [14] A. Petrovskaya and S. Thrun "Model based vehicle detection and tracking for autonomous urban driving" Autonomous Robots, Volume 26 Issue 2-3. April 2009.
- [15] B. Douillard, A. Brooks and F. Ramos "A 3D Laser and Vision Based Classifier International Conference in Intelligent Sensors, Sensor Networks and Information Processing (ISSNIP) 2009.
- [16] D. Steinhauser, O. Ruepp and D. Burschka "Motion segmentation and scene classification from 3D LIDAR data" Intelligent Vehicles Symposium, IEEE. 2008.